Full paper

Dendrite-free lithium metal solid battery with a novel polyester based triblock copolymer solid-state electrolyte

Bohao Zhang [a], Yulong Liu [a], Xiumei Pan [a], Jia Liu [a], Kieran Doyle-Davis [b], Liqun Sun [a], Jun Liu [a], Xuefeng Jiao [a], Jing Jie [a], Haiming Xie [a,**], Xueliang Sun [b,*]

[a] National & Local United Engineering Laboratory for Power Battery, Department of Chemistry, Northeast Normal University Changchun, 130024, China
[b] Department of Mechanical and Materials Engineering, University of Western Ontario, London, ON, N6A 5B9, Canada

A B S T R A C T

Solid-state polymer Li metal batteries have been regarded as a promising candidate for next-generation batteries due to their high-energy densities provided by the Li metal and the improved safety provided by the solid electrolyte. Polyester is one attractive polymer host, which could be an alternative to polyether-based solid electrolyte due to its excellent lithium ion transport ability and wide electrochemical stability window. Here, a BAB-type triblock copolymer is synthesized with poly (propylene carbonate) as A-block and poly (ε-caprolactone) as B-block. The triblock copolymer electrolyte exhibits a high ionic conductivity of 3×10^{-5} S cm^{-1} at 30 °C with a high lithium ion transference number (0.4) and an extremely wide electrochemical window (5 V). A highly stable interface against Li metal is maintained for more than 760 h at a current density of 0.1 mA cm^{-2}. A LiFePO$_4$ cathode based solid state battery delivers a high discharge capacity of 142 mA h g^{-1} at 0.05C, room temperature, and 161 mA h g^{-1} at 0.1C, 70 °C with a capacity retention of 90% after 200 cycles. To understand the excellent electrochemical performance, the morphology and chemical information at both anode and cathode interface are characterized and analyzed. The synthesis of this triblock copolymer demonstrates a new direction in developing high ionic conductivity solid polymer electrolyte for solid-state polymer batteries.

1. Introduction

Rechargeable Lithium ion batteries (LIBs) with large capacity, high voltage, long cycle life, and low self-discharge have attracted extensive attention and have been widely considered as one of the most prominent energy storage systems [1,2]. However, safety problems, arising from the lithium dendrite formation and organic solvents flammability, limit the rapid market expansion of LIBs in both portable electronic devices and electric vehicles (EVs) [3,4]. As such, safety issues drive much of development of all-solid-state lithium batteries using solid-state polymer electrolytes (SPEs) compared to liquid electrolytes. Similarly, Li metal can be used as anode material due to its high theoretical specific capacity of 3860 mA h g^{-1}, which significantly increases the energy density of solid state battery [5,6]. After the pioneering work by Armand et al., solid-state polymer battery research has made enormous progress during last decade [7–9].

Typically, SPEs consist of polymeric matrices which can dissociate a lithium salt. Poly (ethylene oxide) (PEO) is one of the most extensively studied polymer hosts in recent years, as it possesses a high dielectric constant ($\varepsilon_r \approx 5$), strong Li$^+$ solvating ability and high chain flexibility [10]. However, the drawbacks of PEO-based SPEs, such as low lithium ion transference number (0.1–0.3), low ionic conductivity at room temperature ($\approx 10^{-7}$ S cm^{-1}), and narrow electrochemical stability window (<4.0 V vs. Li$^+$/Li), limit the further improvement of energy density for all-solid-state lithium batteries [11,12]. In order to address the above-mentioned issues, some alternative host materials have been proposed, such as poly (vinylene carbonate) (PVC), poly (ethylene carbonate) (PEC) and polyacrylonitrile (PAN) [13–15].

Poly (ε-caprolactone) (PCL), an ester-based polymer, is a promising host material as a SPE. C.P. Fonseca et al. used PCL as SPE in solid state batteries for the first time in 2006 [16]. As a flexible chain, PCL demonstrates a strong Li$^+$−solvating capability, a low glass transition temperature (T_g) at −60 °C and a large electrochemical stability window up to 5 V vs. Li$^+$/Li [17,18]. Like most of the polymer matrices, PCL also

---

* Corresponding author.
** Corresponding author.
E-mail addresses: xiehm136@nenu.edu.cn (H. Xie), xsun@eng.uwo.ca (X. Sun).

presents some drawbacks. For instance, PCL is a semi-crystalline polyester with a melting process between 40 °C and 66 °C, which limits its ionic conductivity and allows for using as a SPE only at high temperature [19]. To change the semi-crystallinity, many strategies have been utilized including the addition of a plastic phase [20], the synthesis of grafted polymers [21], the incorporation of nanoparticles into the polymer [22,23] and the synthesis of copolymer [24–26]. Synthesis of a copolymer is an effective method to improve the performances of SPEs and has been widely used in PEO-based SPEs [27–29]. A copolymer can link two chemically dissimilar blocks by covalent bonding, combining the properties of individual homopolymers.

In this work, we designed a BAB-type triblock copolymer (TBC) using PCL as the B-block and poly(propylene carbonate) (PPC) as the A-block. PPC has been widely studied and used as a SPE, its amorphous phase leads to a high ionic conductivity [30,31]. The crystallinity of TBC is tuned through the introduction of PPC block, leading to a high ionic conductivity (0.03 mS cm^{-1}) at 30 °C with a high lithium transference number (t_{Li+} = 0.4). Meantime, the electrochemical window of PCL-PPC-PCL is up to 5 V, a significant improvement over PEO-based electrolytes. The PCL-PPC-PCL SPE demonstrates a weaker binding energy than PEO-based electrolytes proved by theoretical calculations, leading to a higher lithium ion transference number. Furthermore, stable Li plating/stripping for 760 h is achieved at 70 °C under a current density of 0.1 mA cm^{-2}. No dendritic Li growth is observed after long cycles due to the formation of a stable interface layer. A LiFePO$_4$ cathode based solid battery delivers a high discharge capacity of 142 mA h g^{-1} at 0.05C, room temperature, and 161 mA h g^{-1} at 0.1C, 70 °C. Stable interface layers formed between the SPE and electrodes are also detected, which are favorable for long term cycling. This triblock copolymer provides both improved safety and improved energy density to be a candidate for the widespread adoption of solid state Li metal batteries.

2. Experimental section

2.1. Materials

Stannous octanoate (Sn(Oct)$_2$, 95%) and ε-caprolactone (ε-CL, 99%) were purchased from Aladdin Reagent Corp. Poly (propylene carbonate) (PPC, M_n = 3000 g mol^{-1}) terminated with hydroxyl groups was purchased from Dazhi Environmental Protection Technology Corp. Lithium bis (trifluoromethanesulfonyl) imide (LiTFSI, Solvay, electrochemical grade) and glass microfiber (GE Healthcare UK Limited)/PE separator (Hong Tu Separator Limited) were dehydrated at 120 °C under vacuum for 24 h. Poly (ε-caprolactone) (PCL, M_n = 10000 g mol^{-1}) was purchased from Aldrich Corp. All chemicals mentioned above were stored in a glovebox (H$_2$O and O$_2$ < 0.1 ppm) after drying. The tetrahydrofuran (THF), anhydrous toluene, anhydrous acetonitrile and petroleum ether were used as received.

2.2. Synthesis of PCL-PPC-PCL

The PCL-PPC-PCL was synthesized by ring-opening polymerization (ROP). With the presence of Sn(Oct)$_2$ catalyst, hydroxyl terminated PPC was used as initiator to trigger ε-CL ring-opening reaction. PPC (0.67 mmol), ε-CL (26.3 mmol), Sn(Oct)$_2$ (0.05 mmol) and 50 ml anhydrous toluene were added into a round-bottom flask equipped with water-cooled condenser and a magnetic stirrer. After purging with argon for 30 min, the polymerization reaction was conducted at 120 °C for 40 h. Subsequently, the crude product was dissolved in THF, and the resultant solution was precipitated into an excess of petroleum ether. Finally, polymers were dried under vacuum at room temperature. Another molecular weight of PCL-PPC-PCL was also prepared with different molar ratio of 6.67/1 (PPC/ε-CL). The two kinds of triblock copolymer PCL-PPC-PCL with similar molecular weight of the PPC central-block (M_n = 3000 g mol^{-1}) and different molecular weights of the PCL end-blocks, i.e. 4300 and 13 431 g mol^{-1} were named as TBC$_{7.3k}$, TBC$_{16k}$ hereafter.

2.3. Polymer electrolyte preparation

To obtain polymer electrolyte membrane, different ratios (10 wt%, 20 wt%, 30 wt%) of LiTFSI and PCL-PPC-PCL were dissolved in anhydrous acetonitrile under argon atmosphere. The mixture was stirred for 24 h to form a homogeneous solution. After that, the solution was casted onto glass microfiber or polyethylene (PE) separator, following by evaporating and drying at 60 °C under high vacuum conditions for 48 h. Li salt-doped PCL (PCL-SPE) and PPC were also prepared as polymer electrolytes. PPC was casted onto glass microfiber named as GPPC-SPE.

2.4. Materials characterization

Nuclear magnetic resonance (NMR) with a Bruker Avance lll HD 600 MHz was applied to confirm the structure of PCL-PPC-PCL, using chloroform-d (CDCl$_3$) as solvent and tetramethylsilane as internal standard. The Fourier transform infrared (FTIR) spectra were performed at ambient temperature using a Nicolet 6700 spectrometer. The molecular weights (M_n, M_w) and polydispersity indices (PDI, M_w/M_n) of the polymers were measured by TOSOH HLC-8220 gel permeation chromatography (GPC). High-resolution mass spectra (HRMS) were recorded on Bruck microtof. To analyze the phase behavior, X-ray diffraction (XRD) measurements were performed by a Rigaku smartlab diffractometer within a 2θ range of 10–50°. The crystallinity of the sample was calculated using peak separation software Jade 5 according to the equation:

$$\chi_c = \frac{I_c}{I_c + I_a} \tag{1}$$

where I_c represents the total crystalline area and I_a represents the amorphous area. Differential scanning calorimetry (DSC) was measured using a NETZSCH DSC 200F3 with a scan rate of 10 °C min^{-1} under a flowing nitrogen atmosphere. Thermogravimetric analysis (TGA) was acquired on a Henven T15-114, with a heating rate of 10 °C min^{-1}. The morphologies of the rigid backbone, membrane and cycled electrodes were characterized via scanning electron microscopy (SEM) (Hitachi S5500). All the samples for SEM were coated with a very thin gold layer for imaging.

2.5. Electrochemical measurements

Ionic conductivities of the PCL-PPC-PCL polymer electrolytes were measured by electrochemical impedance spectroscopy (EIS). The stainless steel (SS) was used as blocking electrodes to assemble coin cells SS/SPEs/SS. The measurement was carried out from 30 °C to 80 °C. The conductivity was calculated through equation:

$$\sigma = \frac{L}{R_b \times S} \tag{2}$$

where σ is the ionic conductivity of the electrolyte, R_b is the bulk impedance of SPE, L is the thickness of the electrolyte and S is the surface area of the electrolyte. The multiple cyclic voltammetry (CV) and linear sweep voltammetry (LSV) of SPEs were tested with Li/SPEs/SS cells to determine the electrochemical stability. The potential range was between −0.5 V and 6 V versus Li$^+$/Li. To measure the lithium ion transference number (t_{Li+}), an electrochemical technique developed by Bruce et al. was used [32]. The measurements were carried at 70 °C by a combination of AC impedance measurement and DC polarizationmeasurement. The Li/SPEs/Li cells were subjected to 10 mV polarization bias (ΔV). The initial (I_i) and steady (I_s) state currents were recorded. Simultaneously, the initial (R_i) and final (R_s) resistances of the cells were recorded in the frequency range from 0.01–10^6 Hz by applying a 10 mV perturbation. The t_{Li+} was then calculated using the Bruce−Vincent−Evans equation:
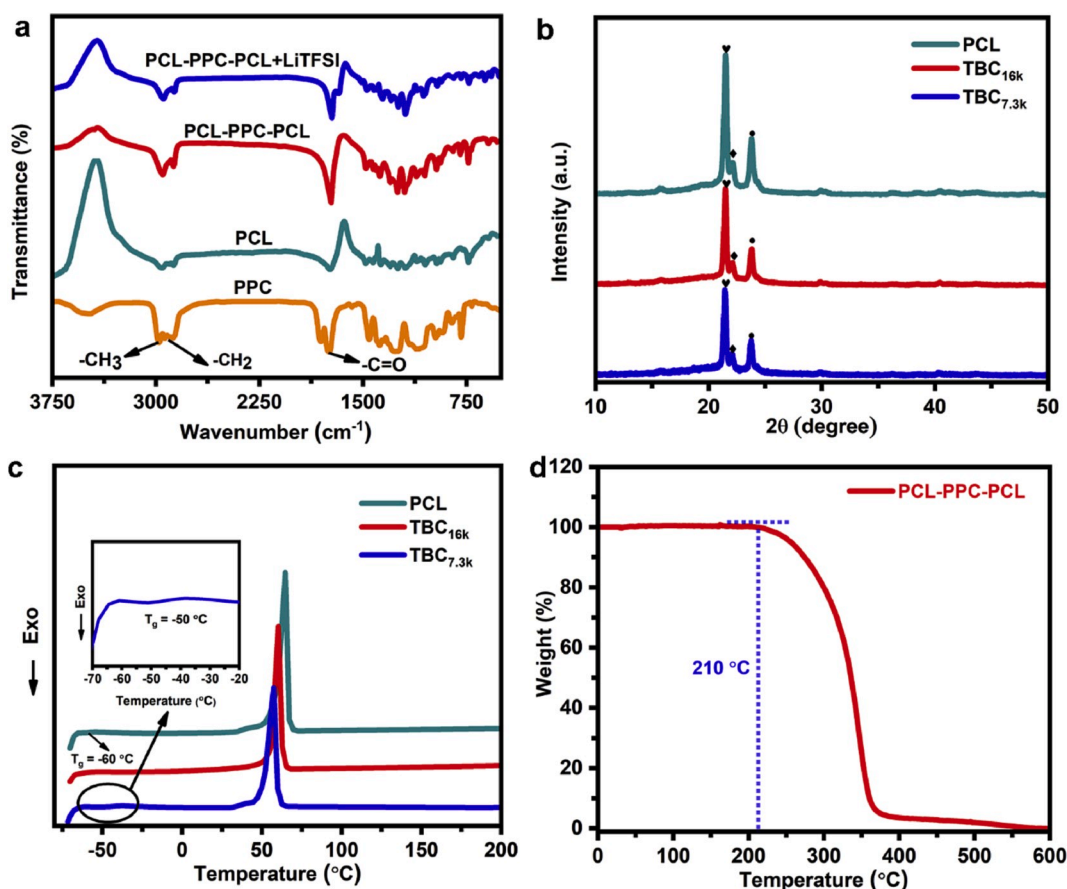
Fig. 1. Physical performances of prepared copolymers. (a) FTIR spectra of PPC, PCL, PCL-PPC-PCL and TBC doped with LiTFSI. (b) XRD patterns and (c) DSC profiles of PCL and TBC samples with different molecular weights. (d) TG curve of TBC.

$$t_{Li+} = \frac{I_s \left(\Delta V - I_i R_i\right)}{I_i (\Delta V - I_s R_s)} \quad (3)$$

The compatibility of PCL-PPC-PCL toward lithium metal was evaluated by monitoring the evolution of the impedance values of Li/SPEs/Li symmetric cells. Polarization tests of the Li/SPEs/Li symmetric cells were employed to investigate the interface between Li and the electrolyte, at a current density of 0.1 mA cm^{-2} (cycling capacity of 0.1 mA h). In order to demonstrate the feasibility of the SPE, all-solid-state polymer batteries were assembled and tested. The LiFePO$_4$ (LFP) and LiNi$_{0.5}$Co$_{0.2}$Mn$_{0.3}$O$_2$ (NCM, suppied by Beijing Easpring Material Techenology Co. LTD.) cathodes were composed of 80 wt% active materials, 10 wt% PVDF, and 10 wt% super P with a mass loading of 1.5 mg.

2.6. Electrode characterization

After long-term charge-discharge tests, the cycled electrodes were disassembled in the glovebox. The chemical information of interfacial compounds was analyzed by X-ray photoelectron spectroscopy (XPS) (ESCALab 220i-XL). All the XPS samples were prepared in the glovebox and sealed in a box. To prevent oxidation, the samples were transferred into XPS machine as quickly as possible. Extensive oxidation upon air exposure cannot, however, be ruled out.

2.7. Calculations

All calculations were carried out using the Gaussian 09 code at the B3LYP/6–311++G (d,p) level to compute various Li$^+$–polymer clusters. The structural optimization was determined by energy minimization based on density functional theory (DFT). The binding energies were

defined as $\Delta E = E$ (Li$^+$−complex) -[E (polymer)+ E (Li$^+$)].

3. Results and discussion

The PCL-PPC-PCL host material was synthesized through bulk ring-opening polymerization of ε-CL, initiated by the hydroxyl end groups of PPC chain (Scheme S1). The NMR spectrum of the PCL-PPC-PCL triblock copolymer is presented in Fig. S1. Comparing with the ^{1}H NMR spectra of pure PCL and PPC (Figs. S1b and S1c), the simultaneous appearance of the characteristic peaks of both PPC and PCL protons in Fig. S1a implies the successful synthesis of PCL-PPC-PCL triblock copolymer.

Fig. 1a displays the Fourier transform infrared (FTIR) spectra of PPC, PCL and PCL-PPC-PCL. The stretching vibration peaks at 2800–2900, 1749 and 1100 cm^{-1}, respectively, are the characteristic absorption of the C–H, C=O, and C–O–C bands originating from PPC. After introducing PCL (only containing –CH$_2$) onto the backbone, the intensity of band associated with the –CH$_2$ stretching vibration between 2900 and 2987 cm^{-1} increases. Meanwhile, the C=O vibration mode has shifted from 1749 to 1724 cm^{-1} in the process because of the shearing vibration of C=O group in the PCL end-block. These spectral feature changes prove successful synthesis of the targeted structure of PCL-PPC-PCL. After doping with LiTFSI salt, a new peak appears at about 1705 cm^{-1}, which belongs to the coordination of Li$^+$− C=O [33,34].

Two different molecular weights of PCL-PPC-PCL were synthesized by controlling both molar ratio of ε-CL/PPC and reaction time. Gel permeation chromatography (GPC) testing was carried out to determine the molecular weights and corresponding polydispersity indices (PDI) of different samples. The molecular weight of TBC$_{7.3k}$ is estimated to be M_n = 7300 g mol^{-1}, and a molar composition of PCL/PPC is 59/41. The
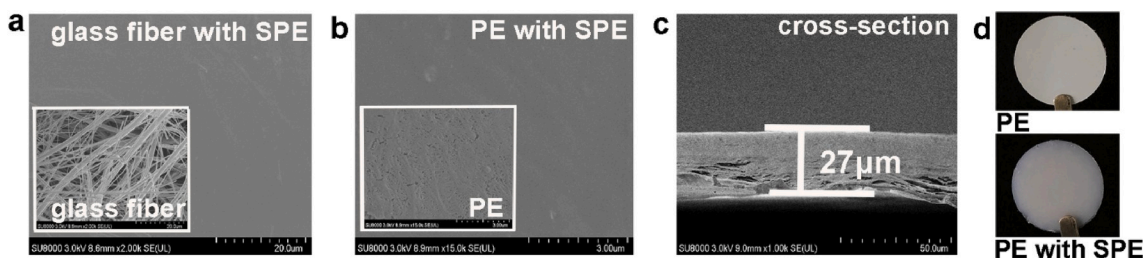
Fig. 2. The morphologies of the SPE electrolyte films. (a) Glass microfiber with SPE (inset shows the pure glass microfiber). (b) PE separator with SPE (inset shows the pure PE separator). (c) The cross-section of PE separator with SPE. (d) Photographs of PE separator and PE separator with SPE.

molecular weight of TBC_{16k} is $M_n = 16\ 431$ g mol^{-1} with a molar composition of 82/18. The PDI is in the range of 1.2–1.6 and the GPC traces are unimodal peaks for both polymers (Fig. S1d), indicating the monodisperse nature of the synthesized triblock copolymer.

Poly (ε-caprolactone) (PCL), similar to PEO, is a semi-crystalline linear aliphatic polyester. As such, the ionic conductivity of PCL based polymer electrolytes is limited by the crystallinity [16,20]. Synthesis of a block copolymer is one effective way to control the crystallinity [35]. The crystallinity of PCL-PPC-PCL copolymers was detected by X-ray diffraction (XRD) and differential scanning calorimetry (DSC). As shown in Fig. 1b, the XRD pattern of pure PCL exhibits typical Bragg reflections at $2\theta = 21°$ (110), 21.2° (111) and 23° (200). Meanwhile, the crystallinity of PPC is very low, and there is no other peak observed except PCL [31]. With the introduction of PPC into the main chain, the peak intensities of TBC decrease obviously. The degree of crystallinity of pure PCL, TBC_{16k} and $TBC_{7.3k}$ are 69.09%, 59.12%, 46.16%, respectively. The crystallinity of PCL phase in TBC slightly increases with the inclusion of

PPC. Taking TBC_{16k} with 82% molar content of PCL for example, the theoretical crystallinity of the crystallizable block in TBC_{16k} should be 72%, which is higher than pure PCL (69.09%). In our opinion, this tendency is reasonable. The presence of PPC can effectively dilute the crystalline content of TBC. Meanwhile, the enhanced segment movement by the dilution effect leads the crystallizable block easier to crystallize [36]. Therefore, the crystallinity of PCL phase in TBC increases. However, we should note that, being used as polymer electrolyte, the decreased crystallinity in global terms of TBC with the inclusion of PPC is still beneficial to improve the ionic conductivity. Simultaneously, PPC can also participate in the transmission of Li^+.

Fig. 1c displays the DSC curves of pure PCL, TBC_{16k} and $TBC_{7.3k}$. For pure PCL, a phase transition is observed at -60 °C which is the glass transition temperature (T_g). Meanwhile, a relatively sharp endothermic peak is detected at 65 °C, indicating the melting temperature (T_m) of pure PCL. The melting point of PCL-based copolymer electrolytes can be depressed by incorporating higher content of comonomer [26]. From
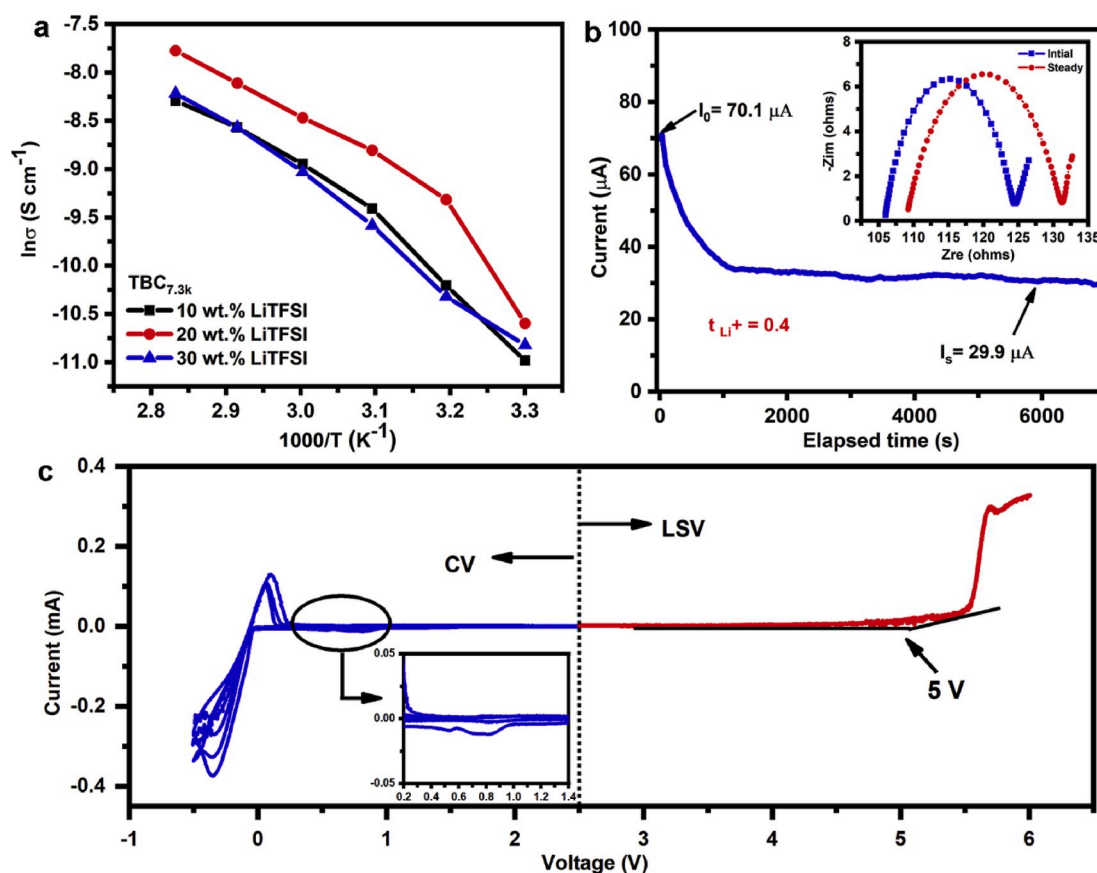
Fig. 3. Electrochemical performances. (a) Temperature dependence of ionic conductivity for $TBC_{7.3k}$ with different ratios of LiTFSI. (b) Polarization curves obtained by chronoamperometry. Inset shows the Nyquist plots of the symmetrical cell in the initial and steady states. (c) Multiple CV cycles and LSV curves of $TBC_{7.3k}$-SPE at 70 °C.
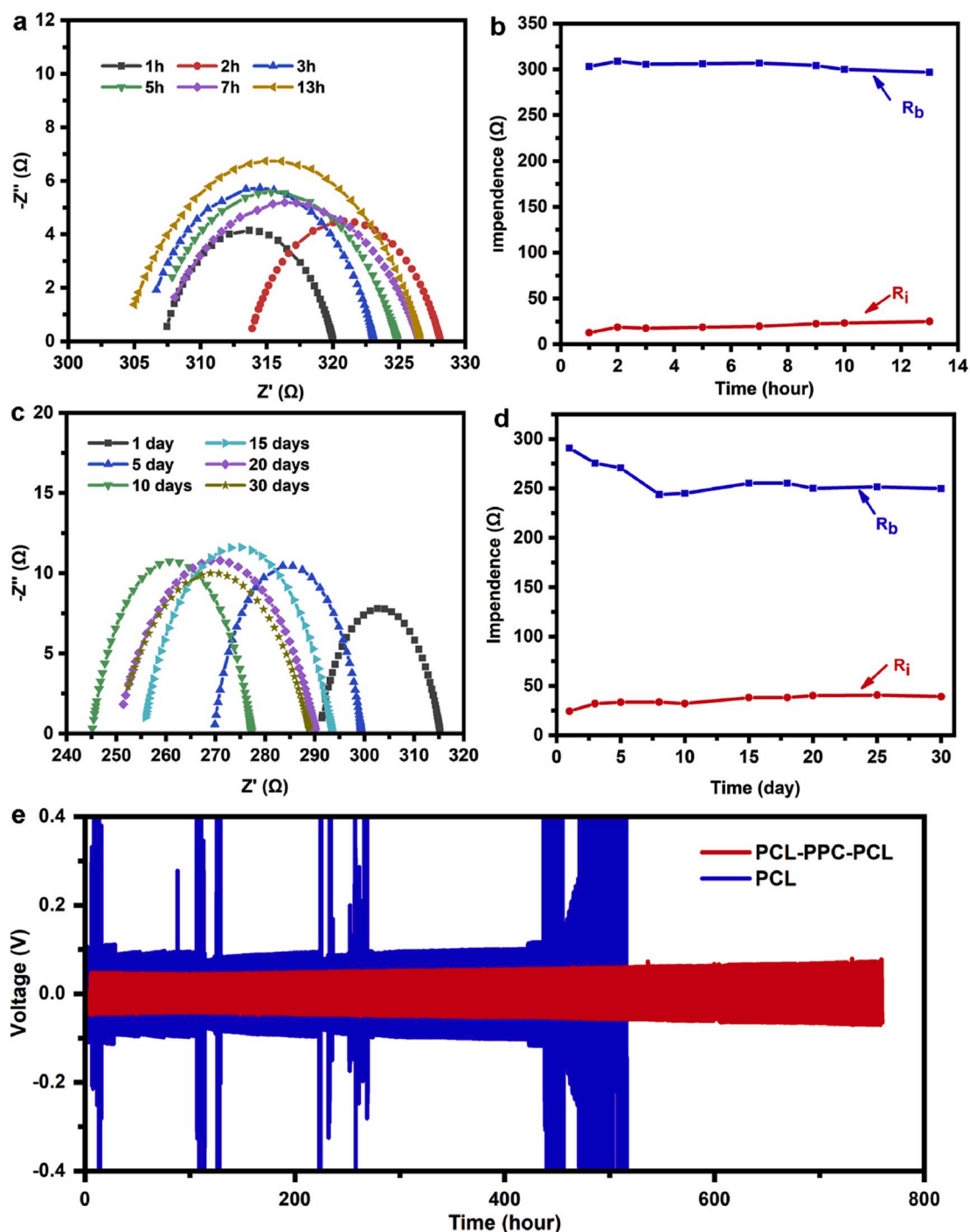
Fig. 4. The electrochemical performances of Li//Li symmetrical cells (a–d) Time evolution of the interfacial resistances of Li/TBC$_{7.3k}$-SPE/Li after various storage times at 70 °C. (e) Galvanostatic tests of Li/TBC$_{7.3k}$-SPE/Li and Li/PCL-SPE/Li cells at a current density of 0.1 mA cm^{-2}.

the DSC results, TBC$_{7.3k}$ contains the lowest melting point (~57 °C) than that of TBC$_{16k}$ (~60 °C) and PCL (~65 °C). These trends are in good agreement with XRD results. Furthermore, a relatively low T_g (−50 °C) can enhance segment movement, making TBC$_{7.3k}$ a promising polymer electrolyte for LIBs. The thermal stability of PCL-PPC-PCL was determined by thermogravimetric analysis (TGA) (Fig. 1d). The triblock copolymer becomes unstable at around 210 °C with weight loss, this relatively high decomposing temperature (well outside any operating temperature) is beneficial to the safety of solid-state battery.

The mechanical properties of the synthesized electrolytes are not adequate for forming free-standing films. Thus, the rigid backbones were used to support electrolytes, and all cell tests were performed with the inclusion of a backbone. The morphologies of the rigid backbones and the electrolyte films are displayed in Fig. 2. The glass microfiber membrane consists of irregularly aligned microfibers and large-sized pores, with the gaps among the backbone mechanically supporting the polymer electrolyte [37,38]. Once the gaps fill with SPEs, a dense and homogenous layer (~200 μm thick) is formed and used as separator for solid-state battery. To achieve higher energy density, ultrathin and lightweight solid electrolyte is an urgent requirement [39]. Hence, a commercialized PE separator is used as support for the copolymer, and a 27 μm thick solid state electrolyte was obtained (Fig. 2b and c). Such a

thin solid polymer electrolyte will guarantee higher energy density based on the drastically reduced volume.

Fig. S2 illustrates the temperature dependence of ionic conductivity of pure PCL, $TBC_{7.3k}$ and TBC_{16k} at various temperatures (ranging from 30 to 80 °C) and concentrations of Li salt. Li salt-doped $TBC_{7.3k}$ exhibits the highest ionic conductivity throughout the tested temperature range, regardless of LiTFSI doping content. The differences in conductivities for the synthesized polymer electrolytes are in line with the crystallinity differences ($TBC_{7.3k}$ has the lowest crystallinity) indicated by the DSC and XRD results. The salt concentration is another critical factor influencing the ionic conductivity. Among all samples, $TBC_{7.3k}$ with 20 wt% salt achieves the maximum conductivity of $\sigma = 3 \times 10^{-5}$ S cm^{-1} at 30 °C and 2.7×10^{-4} S cm^{-1} at 70 °C (Fig. S3). Fig. 3a shows the temperature dependence of ionic conductivity for $TBC_{7.3k}$ with different ratios of LiTFSI. The typical Vogel-Tammann-Fulcher (VTF) behavior is observed in $TBC_{7.3k}$ with 20 wt% LiTFSI at higher temperature (50–80 °C). Thus, the activation energy (E_a) can be calculated by the VTF empirical equation:

$$\sigma = AT^{-1/2}exp\left[\frac{-E_a}{R(T-T_0)}\right] \tag{4}$$

where A is the pre-exponential factor, E_a is the activation energy, R is the ideal gas constant and T_0 is the Vogel scaling temperature related to T_g, at which the free volume disappears. According to equation (4), the E_a for $TBC_{7.3k}$ with 20 wt% LiTFSI in the higher temperature region (50–80 °C) is 4.49 kJ mol^{-1}. This value is much lower than that of other polycarbonate-based polymer electrolytes, such as 28.42 kJ mol^{-1} for PCPU reported by Bao et al. [40], and similar to 4.97 kJ mol^{-1} for PEC-LiFSI-TiO$_2$ prepared by Tominaga et al. [41]. Considering the high ionic conductivity and low activation energy, $TBC_{7.3k}$ with 20 wt% LiTFSI ($TBC_{7.3k}$-SPE) is chosen and used as SPE in solid-state batteries for following characterizations.

The lithium ion transference number plays an important factor for the lithium deposition process in a solid polymer electrolyte. A low t_{Li+} may induce the growth of Li dendrite and raise safety issues, as analyzed by Lu et al. [42]. As shown in Fig. 3b, the current response to the applied static potential polarization drops rapidly from an initial current of ~70 μA and gradually reaches the steady state (I_s = 29.9 μA). The interfacial resistance increases after the chronoamperometry measurement (R_i = 17.91 Ω, R_s = 22.42 Ω). According to equation (3), the lithiumion transference number is calculated to be 0.4, which is much higher than most of multiple ions PEO-based polymer electrolytes. For example, t_{Li+} = 0.265 was achieved for SPE-PEGDMA$_{480}$ [43], t_{Li+} = 0.14 was obtained for PEO/LiFSI as EO/Li$^+$ = 20 at 80 °C [44], and t_{Li+} = 0.38 was reported for SiO$_2$-aerogel-reinforced composite polymer electrolyte [45]. However, the t_{Li+} value of $TBC_{7.3k}$ with 20 wt% is lower than that of PCL-PTMC reported by J. Mindemark et al. [26]. This may be caused by the concentration of Li salt, which is a factor in determining transference number [46]. The reported polymer electrolyte with higher transference number contains a higher Li salt concentration than this work.

Density functional theory (DFT) calculations were employed to investigate the coordination number of Li$^+$−PEO and Li$^+$−PCL-PPC-PCL. As shown in Fig. S4, the coordination number of PCL-PPC-PCL with Li$^+$ is studied for the first time, with coordination number (CN) = 4 shown to be the most stable conformation. In PEO systems, however, a CN of the most stable configuration is 6 proved by P. Johansson [47]. Additionally, the binding energy (ΔE) of Li$^+$−PCL-PPC-PCL complex (ΔE = −107.3 kcal mol^{-1}) and Li$^+$−PEO complex (ΔE = −123.7 kcal mol^{-1}) are calculated. Given the weaker coordination environment of the Li$^+$ and the reduced binding energy in the PCL-PPC-PCL triblock copolymer, it is intuitive that an increased lithium ion transference number is observed experimentally (Fig. 3b).

The electrochemical stability window of PCL-PPC-PCL polymer electrolyte was examined by multiple cyclic voltammetry and linear sweep voltammetry on a stainless-steel working electrode with Li metal as a reference electrode. The cathodic scan shows a couple of reversible redox peaks between −0.2 and 0.2 V versus Li$^+$/Li, corresponding to the lithium plating and stripping process (Fig. 3c). After three cycles, the reduction peaks can be detected at around 0.8 V. These peaks might be associated to degradation products of polymer and TFSI$^-$ formed at the interface, which are similar to the previous reported PCL-based electrolytes and PEO-based electrolytes [45,48]. The polymer with ester/carbonate group has a strong adhesion to Li metal as proved by Ebadi et al. using DFT calculations, which explains the formation of SEI at low potential [49]. Furthermore, there is no obvious oxidation peak until 5 V, which is much higher than both traditional liquid electrolytes (4.5 V) and PEO-based electrolytes (3.7 V). The electrochemical window of PCL-PPC-PCL is wide enough for potential application in high-voltage lithium metal batteries.

The interface stability of SPEs towards Li metal is critical for solid state batteries [50–53]. The interfacial resistance of a symmetric nonblocking Li/$TBC_{7.3k}$-SPE/Li cell was recorded by monitoring the impedance changes as a function of time under 70 °C without applying any currents (Fig. 4a–d). As shown in Fig. 4a and b, no obvious variation in the bulk resistance (R_b) occurs within 13 h at rest, indicating a stable polymer electrolyte. After 7 h, the interface resistance (R_i) increases from 14.4 Ω to 21.2 Ω and becomes stable afterward. This slight change in impedance is caused by the formation of a solid electrolyte interphase (SEI) between the Li-metal anode and the SPE [44]. The slight changes in R_b and R_i of PCL-PPC-PCL in this work differ significantly from other polycarbonate-based electrolytes reported by Cui, such as CPPC-SPE, CPBC-SPE and CPEC-SPE [50]. These phenomena suggest that the PCL end-block on both sides of PPC effectively restrain the contact between PPC and Li-metal electrode, thereby limiting the reaction at the interface. For comparison, the impedances of Li/PCL-SPE/Li and Li/GPPC-SPE/Li were monitored from 1 to 13 h shown in Fig. S5. The R_b of Li/PCL-SPE/Li (Figs. S5a and S5b) changes slightly from 415.1 to 420.1 Ω. But, the R_i increases obviously from 29.87 to 42.82 Ω. These changes are caused by the side reaction between Li metal and SPE [44, 54]. Meanwhile, both R_b (466.8–36.61 Ω) and R_i (32.62–19.98 Ω) of Li/GPPC-SPE/Li (Figs. S5c and S5d) change significantly with time, which are similar to the report by Cui et al. [50]. They ascribed these changes to the side reaction occurred at the interface of Li-metal electrode and PPC, leading to the degradation of the polymer. The by-product of PPC after reacting with Li metal is propylene carbonate, which has been detected by high resolution mass spectrometry (HR-MS) in Cui's group [50]. Longer time-dependent impedance results of Li/$TBC_{7.3k}$-SPE/Li show that the R_b decreases slightly from 290.9 to 245.1 Ω within 7 days and becomes stable (Fig. 4c and d). The slightly reduced bulk resistance is due to the formation of a stable interface between SPE and Li metal. Even after 30 days of testing, no significant change for R_i is presented. The Li/$TBC_{7.3k}$-SPE/Li symmetric cell was disassembled after 30 days. There is no peak at 125.0209 belonging to C$_4$H$_6$O$_3$Na$^+$ detected in PCL-PPC-PCL by the HR-MS, as shown in Fig. S6, an indicator of carbonate dissociation at the Li metal anode. These results indicate a superior interfacial compatibility of $TBC_{7.3k}$-SPE against the lithium metal anode.

To further evaluate the interfacial performance, the symmetric cells of Li/$TBC_{7.3k}$-SPE/Li and Li/PCL-SPE/Li were cycled at a current density of 0.1 mA cm^{-2} at 70 °C. From Fig. 4e, even after long-term cycling (760 h), the charge/discharge voltage curves of Li/$TBC_{7.3k}$-SPE/Li are very stable with a low polarization potential at 0.05 V. However, voltage oscillation is observed during repeated cycling of Li/PCL-SPE/Li, indicating the formation of Li dendrites or unwanted side reactions. The cyclability for a Li//Li symmetric cell with GPPC-SPE was also conducted at the similar condition. As shown in Fig. S7, the overpotential fluctuates during the first 30 h resulting from the side reaction between Li anode and GPPC, which is in good accordance with the results of Li// Li impedance tests (Fig. S5). The overpotential increases gradually with the raising time (100–200 h), indicating that a stable interface between
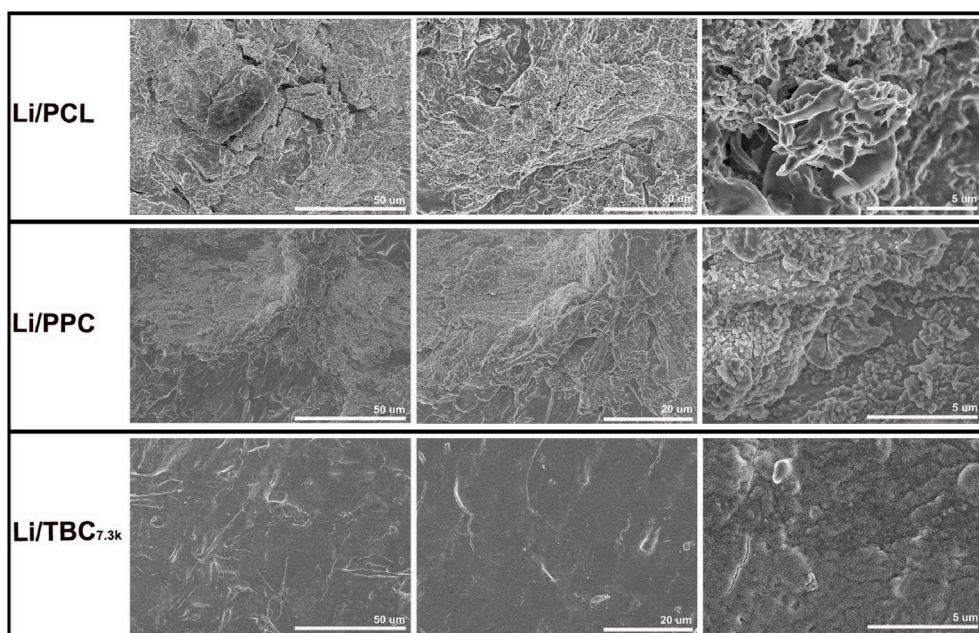
Fig. 5. The SEM images of Li anodes using different electrolytes after 500 h Li//Li cycles.

the Li anode and GPPC-SPE has not achieved. Note that the overpotential maintains stable after 300 h cycles. This could be given an explanation that the small molecule PPC has generated, which has been reported to stabilize the interface between Li and PPC [50]. Therefore, only TBC$_{7.3k}$-SPE demonstrates stable interfacial performance against Li metal, while the SPEs of the constituent polymers in PCL and PPC individually are unstable.

To understand the behavior of Li stripping and plating, the Li//Li symmetric cells using TBC$_{7.3k}$-SPE, PCL-SPE and GPPS-SPE as electrolytes were disassembled after 500 h cycling, and the morphologies of Li anodes were examined by SEM. As Fig. 5 shown, a large amount of "dead Li" and inhomogeneous lithium deposition can be clearly observed in Li/PCL-SPE/Li and Li/GPPC-SPE/Li. However, on the surface of Li metal in Li/TBC$_{7.3k}$-SPE/Li, the lithium deposition is more uniform.

The chemical compositions of SEI on Li anodes for cells using different electrolytes of TBC$_{7.3k}$-SPE, PCL-SPE and GPPC-SPE were examined by XPS after 500 h Li//Li cycling (Fig. S8). For the SEI of TBC$_{7.3k}$-SPE/Li, ROCO$_2$Li (~531.5 eV) and ROLi (~530.2 eV) can be detected in the O 1s spectrum, corresponding to polymer degradation products. This is similar to the previous report published by Sun et al. [55]. Meantime, LiF (~684.7 eV), Li$_3$N (~397.1 eV), Li$_2$O (~528.1 eV), Li$_2$SO$_3$ (~166.7 eV) and Li$_2$S (~160.2 eV) are shown in F 1s, N 1s, O 1s and S 2p spectra, respectively, originating from the Li salt decomposition [56]. Therefore, the SEI layer formed at TBC$_{7.3k}$-SPE/Li interface is consisted of the degradation products of both polymer and Li salt. Compared with chemical compositions on Li anodes for cells with PCL-SPE/Li and GPPC-SPE/Li, higher contents of LiF can be detected on the SEI layer of TBC$_{7.3k}$-SPE/Li. The LiF is an electrical insulator (~10^{-31} S cm^{-1}) which prevents electrons from crossing the SEI layer [57]. Meantime, low diffusing energy and high surface energy of LiF are beneficial to enhance surface diffusion of Li$^+$ during electrodeposition [58]. Thus, this component is favorable to prevent lithium dendrite formation. The SEI components formed in three different electrolytes are summarized in Table S1 for more intuitive comparison.

LiFePO$_4$//Li cells were assembled to evaluated the feasibility of the polymer electrolyte in a solid state battery. For TBC$_{7.3k}$-SPE, the cell maintains a reversible discharge capacity of 151 mA h g^{-1} at 0.1C over 100 cycles, with 99.1% Coulombic efficiency, and a capacity retention of 90% after 200 cycles (Fig. 6a). The long-term cycle performances of TBC$_{7.3k}$-SPE are much better than using pure PCL as SPE. The latter

drops quickly to only 129 mA h g^{-1} after 79 cycles. In addition, room temperature performances of LiFePO$_4$//Li were carried out at 0.05C shown in Fig. 6a. Although the polarization voltage of room temperature is slightly larger than that of the evaluated temperature (70 °C) (Fig. S9a), the discharge capacity is stabilized at about 141.2 mA h g^{-1} for 130 cycles. The result is much higher than PCL-PTMC and PCL doped with nanoparticles under room temperature in the previous literatures [22,26]. Charge–discharge tests at different current densities were examined (Fig. 6c). At 0.1C, 0.2C, 0.4C and 0.5C, the cell displays a specific capacity of 161 mA h g^{-1}, 153 mA h g^{-1}, 139 mA h g^{-1} and 123 mA h g^{-1}, respectively. With the current dropping back down to 0.1C, the capacity recovers to 158 mA h g^{-1}, proving an excellent rate capability. An ultrathin solid polymer electrolyte using PE separator as rigid backbone were also tested at room temperature, which exhibited excellent cycling stability after about 50 cycles of activation (149.8 mA h g^{-1} at 0.05C after 120 cycles) shown in Fig. S9c. The similar activation process occurs in the cell using glass fiber as backbone, which is related to the infiltration of the SPE into the electrode during cycles. Because of the wide electrochemical stability window, LiNi$_{0.5}$Co$_{0.2}$Mn$_{0.3}$O$_2$/TBC$_{7.3k}$-SPE/Li was tested and the results were presented in Fig. S9b. The cell delivers a Coulombic efficiency of 86.5% at the first cycle, and the initial charge and discharge capacity are 166.4 mA h g^{-1} and 144 mA h g^{-1}. However, the Coulombic efficiency is over 95% at the second cycle and maintains over 98% after ten cycles. Thus, this SPE has the potential to be used in high-voltage batteries.

The electrochemical impedance spectroscopy (EIS) measurements of LFP/TBC$_{7.3k}$-SPE/Li and LFP/PCL-SPE/Li were carried out to evaluate resistance change during cycling shown in Fig. S10. There is almost no change for the R_b value of LFP/TBC$_{7.3k}$-SPE/Li cell, indicating a stable TBC$_{7.3k}$-SPE structure during cycling. Although the R_b of LFP/PCL-SPE/Li decreases from 1014 Ω to 540.7 Ω after 60 cycles, the value of R_b is still much higher than LFP/TBC$_{7.3k}$-SPE/Li (371.9 Ω). In addition, both the R_i value of LFP/TBC$_{7.3k}$-SPE/Li and LFP/PCL-SPE/Li increase suggesting that interfacial reactions still occur during long term cycling. Also, the R_i of LFP/PCL-SPE/Li (3066 Ω) is higher than LFP/TBC$_{7.3k}$-SPE/Li (2168 Ω) after 60 cycles, which is consistent with the improved cycling performances of LFP/TBC$_{7.3k}$-SPE/Li compared to LFP/PCL-SPE/Li (Fig. 6a). For better comparison, the electrochemical performances of TBC$_{7.3k}$-SPE and other SPEs are summarized in Table S2.

To examine the interfacial reactions of LFP/TBC$_{7.3k}$-SPE/Li after 200
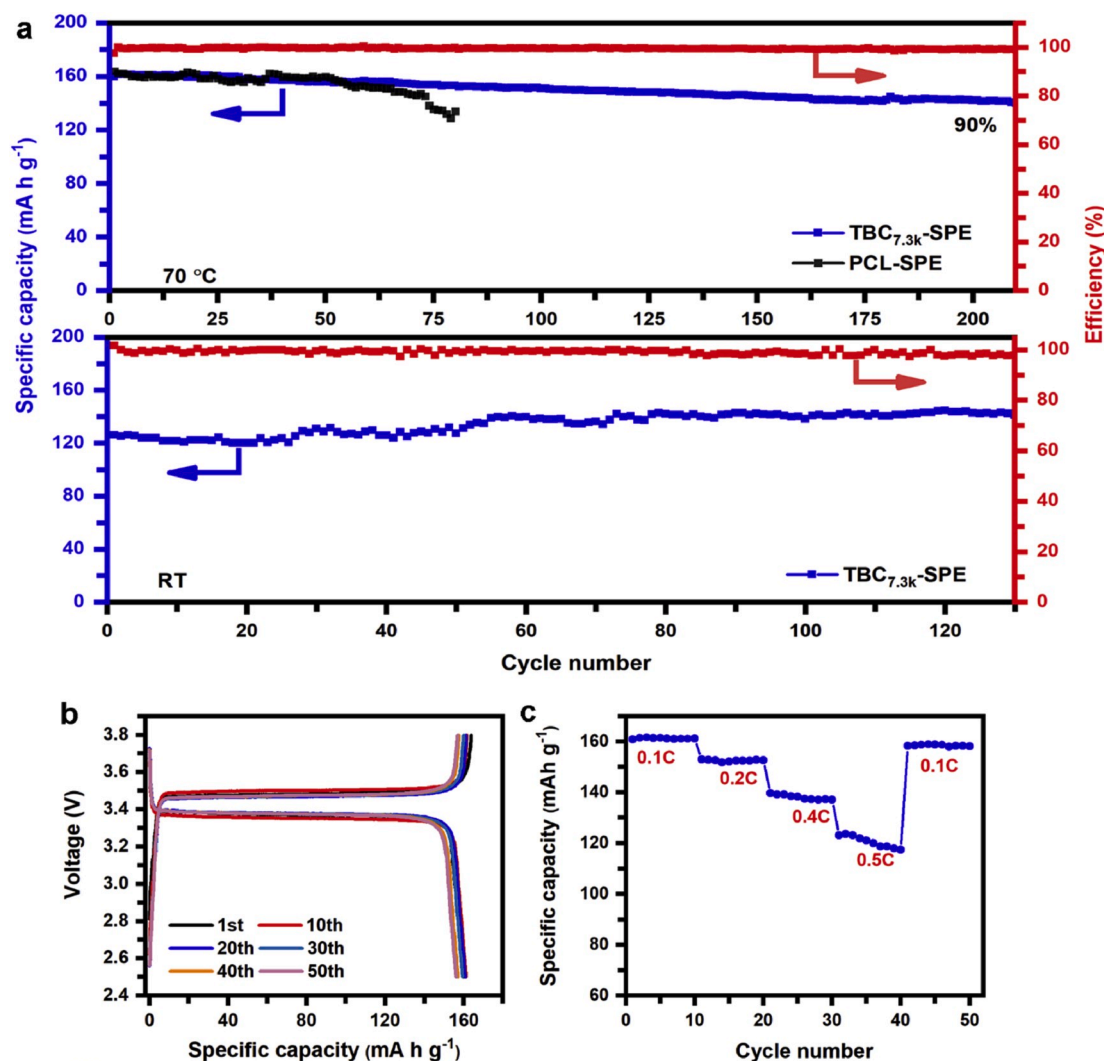
Fig. 6. The electrochemical performances of LFP//Li cells. (a) The long-term cycle performances of TBC$_{7.3k}$-SPE and PCL-SPE at 0.1C, 70 °C (top). The long-term cycle performances of TBC$_{7.3k}$-SPE at 0.05C, room temperature (bottom). (b) Charge-discharge curves at 0.1C of LiFePO$_4$/TBC$_{7.3k}$-SPE/Li cell at 70 °C. (c) Cycle performances at different rates of LiFePO$_4$/TBC$_{7.3k}$-SPE/Li.

cycles, X-ray photoelectron spectroscopy (XPS) and scanning electron microscopy (SEM) were performed to identify physical and chemical information at the interface. Fig. 7 displays the C 1s, F 1s, O 1s, S 2p and N 1s spectra of the LFP cathode and Li anode. For the cathode electrolyte interphase (CEI) shown in Fig. 7a–f, the C 1s spectra can be deconvoluted into four peaks. The sharp peak at ~284.8 eV is the C–C bond. Another peak at ~286.4 eV is attributed to C–O [59] and the CH$_2$ in PVDF [60]. The other two peaks at ~288.9 eV and ~292.6 eV can attribute to O–C$=$O and CF$_3$. The CF$_3$ is associated with the reduction of LiTFSI, which demonstrates that the anion contributes to the formation of the CEI layer [61]. The three main visible components in F 1s spectrum are LiTFSI (~689.4 eV), PVDF (~688.6 eV) and LiF (~684.7 eV), respectively. The O 1s spectrum can be deconvoluted into three peaks. First, Li$_2$CO$_3$ (~532.1 eV) [62] or oxygen atoms bound to carbon with a double bond (~532.0 eV). Second, oxygen bound to carbon with a single bond at ~533.5 eV [63]. Third, the high-energy peak at ~535.9 eV belongs to free TFSI$^-$ adsorbed on the surface of the cathode [64]. The S 2p$_{3/2}$ peak at ~168.4 eV and the N 1s peak at ~399.1 eV, all correspond to the LiTFSI salt. Meanwhile, the salt degradation product Li$_2$SO$_3$ can be found at ~166.7 eV [56]. After long term cycling, the CEI film is mainly consisted of LiTFSI salt decomposition productions and TFSI$^-$ adsorption. The reduction of the polymer and/or side-reactions with LFP particles are not detected from XPS results, contrary to previously

reported results [51]. Furthermore, SEM image of the LFP electrode shows only stable CEI film formed on the surface, no side reactions are probed at the cathode interface.

After long cycles, only some little Li particles are seen in the SEM image shown in Fig. 7g. No dendritic Li growth and mossy Li are observed, which ensures the safety of the solid-state battery. XPS results of the solid electrolyte interphase (SEI) layer between Li metal and SPE are displayed in Fig. 7 (h-l). The C 1s spectrum can be deconvoluted into five peaks. Most of the peaks are similar to the C 1s of CEI except for the low-energy peak at ~283.1 eV, which is assigned to lithium carbide species [65,66]. In the F 1s spectrum, an obvious LiF peak (~684.7 eV) can be detected. LiF can effectively protect Li anode by preventing the electrons from crossing the SEI layer [67]. As for the O 1s spectrum, two new peaks appear at lower binding energy of ~528.1 eV and ~530.2 eV belonging to Li$_2$O and Li$_x$SiO$_y$, respectively. These two compounds are the reaction products of lithium with glass fiber after long charge-discharge cycles [68]. The salt degradation products of Li$_2$SO$_3$ (~166.7 eV) and Li$_3$N (~397.1 eV) can be observed in S 2p$_{3/2}$ and N 1s spectra, respectively [56]. The as-decomposed SEI layer is enriched with a high content of LiF, which is stable chemical compound protecting Li metal from further reduction. This gives rise to long term stable performance of LFP//Li cell. Analyses of a cycled cell suggest that stable interface layers are formed at both cathode side and anode side, as
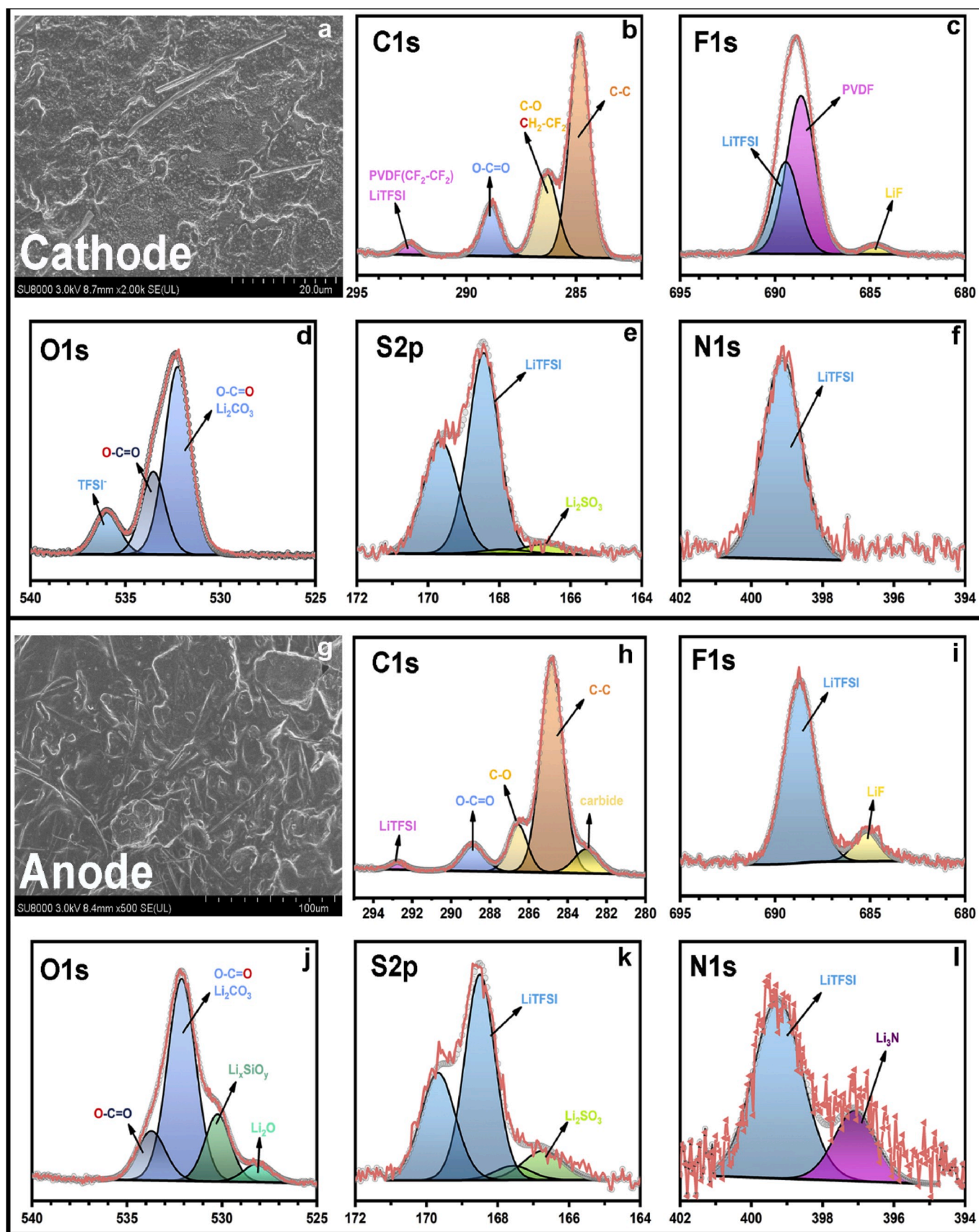
Fig. 7. Post analysis of cycled Li metal solid-state battery. (a–f) SEM and ex situ XPS characterizations on the LFP (top) and (g–l) Li metal anode (bottom) after 200 cycles.
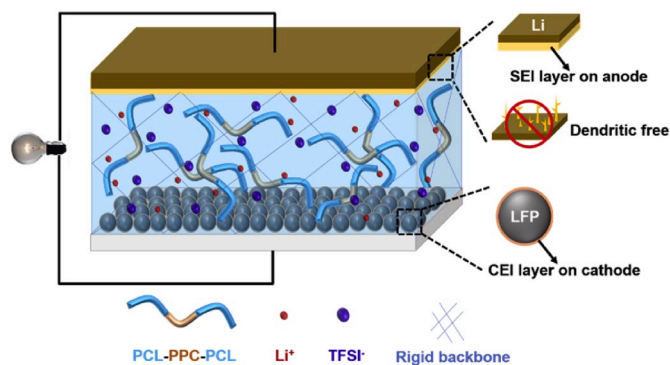
Fig. 8. Schematic illustration of Li metal solid state battery with triblock copolymer electrolyte and stable interfaces.

demonstrated in Fig. 8. Especially, the formation of LiF at lithium metal surface is very helpful in preventing lithium dendrite formation.

4. Conclusion

In summary, a novel triblock copolymer PCL-PPC-PCL has been designed as a host for solid polymer electrolyte. It possesses depressed crystallinity compared with that of PCL. TBC$_{7.3k}$-SPE exhibits a more stable interface towards Li metal than previously reported polycarbonate-based polymer electrolytes. The high lithium ion transference number of TBC$_{7.3k}$-SPE is evidenced by DFT calculations. LFP/TBC$_{7.3k}$-SPE/Li cells display excellent cycling stability and rate capability at both high temperature and room temperature. Interface characterizations between SPE and electrodes suggest that a high fluorinated SEI is formed, which is favorable for long term cycling. This novel SPE is very competitive with other polymer electrolytes for development of next-generation all-solid-state batteries.

Declaration of competing interest

The authors declare that they have no known competing financial interests or personal relationships that could have appeared to influence the work reported in this paper.

CRediT authorship contribution statement

Bohao Zhang: Conceptualization, Software, Formal analysis, Investigation, Writing - original draft. **Yulong Liu:** Formal analysis, Writing - review & editing. **Xiumei Pan:** Methodology, Formal analysis. **Jia Liu:** Validation, Software. **Kieran Doyle-Davis:** Visualization, Writing - review & editing. **Liqun Sun:** Supervision. **Jun Liu:** Resources. **Xuefeng Jiao:** Software. **Jing Jie:** Data curation. **Haiming Xie:** Funding acquisition, Resources. **Xueliang Sun:** Project administration, Resources.

Acknowledgements

Appendix A. Supplementary data

Supplementary data to this article can be found online at https://doi.org/10.1016/j.nanoen.2020.104690.

References

[1] J.B. Goodenough, K.-S. Park, J. Am. Chem. Soc. 135 (2013) 1167–1176.
[2] M. Armand, J.M. Tarascon, Nature 451 (2008) 652–657.
[3] J.B. Goodenough, Y. Kim, Chem. Mater. 22 (2010) 587–603.
[4] A. Mauger, M. Armand, C.M. Julien, K. Zaghib, J. Power Sources 353 (2017) 333–342.
[5] M.-H. Ryou, Y.M. Lee, Y. Lee, M. Winter, P. Bieker, Adv. Funct. Mater. 25 (2015) 834–841.
[6] Z. Zhang, Y. Shao, B. Lotsch, Y.-S. Hu, H. Li, J. Janek, L.F. Nazar, C.-W. Nan, J. Maier, M. Armand, L. Chen, Energy Environ. Sci. 11 (2018) 1945–1976.
[7] M. Armand, Solid State Ionics 9–10 (1983) 745–754.
[8] H. Zhang, J. Zhang, J. Ma, G. Xu, T. Dong, G. Cui, Electrochem. Energy Rev. 2 (2019) 128–148.
[9] S.-J. Tan, X.-X. Zeng, Q. Ma, X.-W. Wu, Y.-G. Guo, Electrochem. Energy Rev. 1 (2018) 113–138.
[10] Z. Xue, D. He, X. Xie, J. Mater. Chem. A 3 (2015) 19218–19253.
[11] D.R. Payne, P.V. Wright, Polymer 23 (1982) 690–693.
[12] M.B. Armand, Annu. Rev. Mater. Sci. 16 (1986) 245–261.
[13] X. Wei, D.F. Shriver, Chem. Mater. 10 (1998) 2307–2308.
[14] K. Kimura, H. Matsumoto, J. Hassoun, S. Panero, B. Scrosati, Y. Tominaga, Electrochim. Acta 175 (2015) 134–140.
[15] H.-K. Yoon, W.-S. Chung, N.-J. Jo, Electrochim. Acta 50 (2004) 289–293.
[16] C.P. Fonseca, D.S. Rosa, F. Gaboardi, S. Neves, J. Power Sources 155 (2006) 381–384.
[17] C.P. Fonseca, S. Neves, J. Power Sources 159 (2006) 712–716.
[18] M. Ravi, S. Song, K. Gu, J. Tang, Z. Zhang, Mater. Sci. Eng. B 195 (2015) 74–83.
[19] X. Wang, H. Zhao, L.-S. Turng, Q. Li, Ind. Eng. Chem. Res. 52 (2013) 4939–4949.
[20] D. Zhang, L. Zhang, K. Yang, H. Wang, C. Yu, D. Xu, B. Xu, L.M. Wang, ACS Appl. Mater. Interfaces 9 (2017) 36886–36896.
[21] L. Imholt, D. Dong, D. Bedrov, I. Cekic-Laskovic, M. Winter, G. Brunklaus, ACS Macro Lett. 7 (2018) 881–885.
[22] T. Eriksson, J. Mindemark, M. Yue, D. Brandell, Electrochim. Acta 300 (2019) 489–496.
[23] X. Yang, Q. Sun, C. Zhao, X. Gao, K.R. Adair, Y. Liu, J. Luo, X. Lin, J. Liang, H. Huang, L. Zhang, R. Yang, S. Lu, R. Li, X. Sun, Nano Energy 61 (2019) 567–575.
[24] P. Zhang, H. Huang, T. He, Z. Hu, ACS Macro Lett. 1 (2012) 1007–1011.
[25] J. Huang, Z.-Z. Tong, B. Zhou, J.-T. Xu, Z.-Q. Fan, Polymer 55 (2014) 1070–1077.
[26] J. Mindemark, B. Sun, E. Törmä, D. Brandell, J. Power Sources 298 (2015) 166–170.
[27] R. Bouchet, S. Maria, R. Meziane, A. Aboulaich, L. Lienafa, J.P. Bonnet, T.N. Phan, D. Bertin, D. Gigmes, D. Devaux, R. Denoyel, M. Armand, Nat. Mater. 12 (2013) 452–457.
[28] R. Bouchet, T.N.T. Phan, E. Beaudoin, D. Devaux, P. Davidson, D. Bertin, R. Denoyel, Macromolecules 47 (2014) 2659–2665.
[29] M. Chintapalli, T.N.P. Le, N.R. Venkatesan, N.G. Mackay, A.A. Rojas, J.L. Thelen, X.C. Chen, D. Devaux, N.P. Balsara, Macromolecules 49 (2016) 1770–1780.
[30] H. Yue, J. Li, Q. Wang, C. Li, J. Zhang, Q. Li, X. Li, H. Zhang, S. Yang, ACS Sustain. Chem. Eng. 6 (2017) 268–274.
[31] J. Zhang, J. Zhao, L. Yue, Q. Wang, J. Chai, Z. Liu, X. Zhou, H. Li, Y. Guo, G. Cui, L. Chen, Adv. Energy Mater. 5 (2015) 1501082.
[32] J. Evans, C.A. Vincent, P.G. Bruce, Polymer 28 (1987) 2324–2328.
[33] J. Mindemark, S. Tang, H. Li, L. Edman, Adv. Funct. Mater. 28 (2018) 1801295.
[34] B. Sun, J. Mindemark, E.V. Morozov, L.T. Costa, M. Bergman, P. Johansson, Y. Fang, I. Furo, D. Brandell, Phys. Chem. Chem. Phys. 18 (2016) 9504–9513.
[35] B. Zhang, Y. Zhang, N. Zhang, J. Liu, L. Cong, J. Liu, L. Sun, A. Mauger, C. M. Julien, H. Xie, X. Pan, J. Power Sources 428 (2019) 93–104.
[36] S. Nojima, Y. Higaki, K. Kaetsu, R. Ishige, N. Ohta, H. Masunaga, T. Hirai, K. Kojio, A. Takahara, Polymer 116 (2017) 403–411.
[37] G. Li, X. Chen, L. Miao, J. Chen, J. Zheng, J. Power Sources 394 (2018) 26–34.
[38] P. Hu, Y. Duan, D. Hu, B. Qin, J. Zhang, Q. Wang, Z. Liu, G. Cui, L. Chen, ACS Appl. Mater. Interfaces 7 (2015) 4720–4727.
[39] J. Wan, J. Xie, X. Kong, Z. Liu, K. Liu, F. Shi, A. Pei, H. Chen, W. Chen, J. Chen, X. Zhang, L. Zong, J. Wang, L.-Q. Chen, J. Qin, Y. Cui, Nat. Nanotechnol. 14 (2019) 705–711.
[40] J. Bao, G. Shi, C. Tao, C. Wang, C. Zhu, L. Cheng, G. Qian, C. Chen, J. Power Sources 389 (2018) 84–92.
[41] Y. Tominaga, K. Yamazaki, Chem. Commun. 50 (2014) 4448–4450.
[42] Y. Lu, M. Tikekar, R. Mohanty, K. Hendrickson, L. Ma, L.A. Archer, Adv. Energy Mater. 5 (2015) 1402073.
[43] Z. Wei, Z. Zhang, S. Chen, Z. Wang, X. Yao, Y. Deng, X. Xu, Energy Storage Mater. 22 (2019) 337–345.
[44] H. Zhang, C. Liu, L. Zheng, F. Xu, W. Feng, H. Li, X. Huang, M. Armand, J. Nie, Z. Zhou, Electrochim. Acta 133 (2014) 529–538.
[45] D. Lin, P.Y. Yuen, Y. Liu, W. Liu, N. Liu, R.H. Dauskardt, Y. Cui, Adv. Mater. 30 (2018) 1802661.
[46] L. Edman, M.M. Doeff, A. Ferry, J. Kerr, L.C. De Jonghe, J. Phy. Chem. B 104 (2000) 3476–3480.
[47] P. Johansson, Polymer 42 (2001) 4367–4373.

[48] A. Bergfelt, M.J. Lacey, J. Hedman, C. Sångeland, D. Brandell, RSC Adv. 8 (2018) 16716–16725.
[49] M. Ebadi, C. Marchiori, J. Mindemark, D. Brandell, C.M. Araujo, J. Mater. Chem. A 7 (2019) 8394–8404.
[50] C. Wang, H. Zhang, J. Li, J. Chai, S. Dong, G. Cui, J. Power Sources 397 (2018) 157–161.
[51] J. Li, S. Dong, C. Wang, Z. Hu, Z. Zhang, H. Zhang, G. Cui, J. Mater. Chem. A 6 (2018) 11846–11852.
[52] C. Wang, K.R. Adair, J. Liang, X. Li, Y. Sun, X. Li, J. Wang, Q. Sun, F. Zhao, X. Lin, R. Li, H. Huang, L. Zhang, R. Yang, S. Lu, X. Sun, Adv. Funct. Mater. 29 (2019) 1900392.
[53] Y. Liu, Q. Sun, Y. Zhao, B. Wang, P. Kaghazchi, K.R. Adair, R. Li, C. Zhang, J. Liu, L. Y. Kuo, Y. Hu, T.K. Sham, L. Zhang, R. Yang, S. Lu, X. Song, X. Sun, ACS Appl. Mater. Interfaces 10 (2018) 31240–31248.
[54] G.B. Appetecchi, S. Passerini, J. Electrochem. Soc. 149 (2002) A891–A897.
[55] B. Sun, C. Xu, J. Mindemark, T. Gustafsson, K. Edström, D. Brandell, J. Mater. Chem. A 3 (2015) 13994–14000.
[56] C. Xu, B. Sun, T. Gustafsson, K. Edström, D. Brandell, M. Hahlin, J. Mater. Chem. A 2 (2014) 7256–7264.
[57] J. Pan, Y.-T. Cheng, Y. Qi, Phys. Rev. B 91 (2015) 134116.
[58] Y. Lu, Z. Tu, L.A. Archer, Nat. Mater. 13 (2014) 961.
[59] H. Ago, T. Kugler, F. Cacialli, W.R. Salaneck, M.S.P. Shaffer, A.H. Windle, R. H. Friend, J. Phys. Chem. B 103 (1999) 8116–8121.
[60] S. Verdier, L.E. Ouatani, R. Dedryvère, F. Bonhomme, b.P. Biensan, D. Gonbeau, J. Electrochem. Soc. 154 (2007) A1088–A1099.
[61] J. Alvarado, M.A. Schroeder, T.P. Pollard, X. Wang, J.Z. Lee, M. Zhang, T. Wynn, M. Ding, O. Borodin, Y.S. Meng, K. Xu, Energy Environ. Sci. 12 (2019) 780–794.
[62] A.T. Appapillai, A.N. Mansour, J. Cho, Y. Shao-Horn, Chem. Mater. 19 (2007) 5748–5757.
[63] U. Zielke, K.J. Hüttinger, W.P. Hoffman, Carbon 34 (1996) 983–998.
[64] Z. Liu, G. Li, A. Borodin, X. Liu, Y. Li, F. Endres, J. Phys. Chem. C 123 (2019) 10325–10332.
[65] A. Schechter, D. Aurbach, H. Cohen, Langmuir 15 (1999) 3334–3342.
[66] Q. Zhao, Y. Zhang, G. Sun, L. Cong, L. Sun, H. Xie, J. Liu, ACS Appl. Mater. Interfaces 10 (2018) 26312–26319.
[67] X.-Q. Zhang, X.-B. Cheng, X. Chen, C. Yan, Q. Zhang, Adv. Funct. Mater. 27 (2017) 1605989.
[68] B. Philippe, R. Dedryvère, M. Gorgoi, H. Rensmo, D. Gonbeau, K. Edström, Chem. Mater. 25 (2013) 394–404.

Xiumei Pan is a professor at Northeast Normal University, P.R. China. She received her Bachelor, Master and Ph.D. degrees in 1991, 1994 and 2002 from Northeast Normal University, respectively. She is a senior research scholar of University of California, Los Angeles in 2017 and a visitor scholar of California State University, Fullerton in 2009–2010. Her current research interests include the theoretical and experiment researches of the lithium ion batteries, the degradation mechanism and kinetics of the volatile organic compounds and the formation mechanism of the new particles.
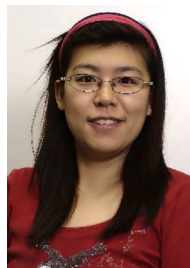
Jia Liu received her M.S. degree from Nano Science & Technology Research Center in Shanghai University and Ph.D degree at the Department of chemistry- Ångström Laboratory in Uppsala University. She is a lecturer in Department of Chemistry of Northeast Normal University. Her research interest lies in a broad aspect of energy storage and conversation systems including Li-ion and Li–O$_2$ batteries, ranging from materials synthesis to the whole-cell characterizations.

Kieran Doyle-Davis received his Honours BSc in Physics from McMaster University in 2018, with research focus on process optimization for lithium ion battery fabrication, and thin polymer films. Kieran is currently an MESc candidate at the University of Western Ontario under the supervision of Prof. Xueliang Sun. His current research interests include the development of next generation surface modified 3-D current collectors for both solution and solid state lithium ion batteries.

Bohao Zhang is currently a Ph.D. candidate in Prof. Haiming Xie's group at Northeast Normal University, China. His current interests focus on the design and synthesis of solid polymer electrolyte for lithium metal batteries.

Liqun Sun received her Ph.D. degree in physical chemistry from Northeast Normal University in 2012. Her current research interests focus on heat-resistant high safety separator for lithium ion batteries and high voltage all solid-state electrolytes for lithium metal batteries.

Yulong Liu is currently associate professor at Northeast Normal University, China. Before working at Northeast Normal University, he was a postdoctoral fellow in Prof. Xueliang (Andy) Sun' Nanomaterials and Energy Group at the University of Western Ontario, Canada. He received his Bachelor degree from Central South University, China, in 2010, and Master degree in 2013. In 2018, he obtained his Ph.D. degree in Materials Science and Engineering from University of Western Ontario. Previously, he worked together with GLABAT Solid State Battery Inc. on commercializing solid state batteries. His current research interests include nanomaterials for lithium ion batteries and the development of the high energy density solid-state batteries.

Jun Liu received his bachelor's degree in 2002 at the Department of Chemistry, Northeast Normal University, China. After obtaining his Ph.D. in 2007 at the same university, Jun Liu spent one year as a postdoctoral fellow with Prof. Petri Pihko at the University of Jyvaskyla, Finland. Currently he is working at Northeast Normal University as associate professor, where his research interests involve functionlized polymers and polymer electrolytes.

Xuefeng Jiao is currently pursuing her M.S. degree under the supervision of Professor Xiumei Pan in Department of Chemistry at Northeast Normal University. Her research interests mainly focus on quantum chemical calculations of solid polymer electrolytes.

Haiming Xie is a professor of Department of Chemistry at the Northeast Normal University and the director of National & Local United Engineering Laboratory for Power Battery. He received his Ph.D. degree from Northeast Normal University in 2008. His main research interests include lithium iron phosphate cathode materials and heat-resistant separators for high safety and high-power lithium ion batteries, low-temperature power batteries and all-solid-state electrolytes for lithium batteries.

Jing Jie is currently pursuing her master's degree in Department of Chemistry at Northeast Normal University under the supervision of Prof. Haiming Xie. Her main research interests involve the development of high-performance polymer electrolytes for lithium-ion batteries.

Prof. Xueliang (Andy) Sun is a Canada Research Chair in Development of Nanomaterials for Clean Energy, Fellow of the Royal Society of Canada and Canadian Academy of Engineering and Full Professor at the University of Western Ontario, Canada. Dr. Sun received his Ph.D. in materials chemistry in 1999 from the University of Manchester, UK, which he followed up by working as a postdoctoral fellow at the University of British Columbia, Canada and as a Research Associate at L′ Institut National de la Recherche Scientifique (INRS), Canada. His current research interests are focused on advanced materials for electrochemical energy storage and conversion.